# Towards quasi-DC conductivity of Warm Dense Matter measured by single-shot terahertz spectroscopy[a]

B. K. Ofori-Okai,[1,2,b] A. Descamps,[1] J. Lu,[1] L. E. Seipp,[1,3] A. Weinmann,[1,3] S. H. Glenzer,[1] and Z. Chen[1]

[1] *SLAC National Accelerator Laboratory, 2575 Sand Hill Road, Menlo Park, CA 94025, USA*

[2] *Department of Chemistry, Massachusetts Institute of Technology, 77 Massachusetts Avenue, Cambridge, MA 02139, USA*

[3] *Universität der Bundeswehr München, Werner-Heisenberg-Weg 39, 85579 Neubiberg, Germany*

(Dated: 19 June 2018)

We present an experimental setup capable of measuring of the near DC conductivity of laser generated warm dense matter using single-shot terahertz time-domain spectroscopy. The setup uses a reflective echelon and balanced detection to record THz waveforms with a minimum detectable signal of 0.2% in a single laser pulse. We describe details of the experimental setup and the data analysis procedure, and present single-shot terahertz transmission data on aluminum that has been laser heated to an electron temperature of 0.5 eV.

## I. INTRODUCTION

Warm dense matter (WDM) refers to materials with temperatures between ∼1-100 eV, and densities 0.1-10 times that of a solid[1,2]. Theories from plasma physics usually fail at describing WDM because in this regime the electron energy at Fermi level is comparable to the thermal energy, and the strongly coupled ion system deviates significantly from an ideal gas. One important example where plasma theory fails is the breakdown of the Spitzer conductivity model[3,4]. Because of the importance of the electrical conductivity, especially at zero-frequency (DC), a number of models have been developed to predict the conductivity[4–6] and precise experimental data are needed to test and improve these models. While WDM can be generated in a laboratory using intense femtosecond lasers, laser generated WDM is short-lived, and so ultrafast single-shot diagnostics with picosecond or better temporal resolution are required for probing the material properties. Ultrafast near-infrared and free-electron lasers (FELs) have been used to estimate the DC conductivity from measurements of the AC conductivity at visible frequencies[7–9] and the dynamic conductivity at plasmon frequencies[6,10], but these extrapolations are very model dependent. These highlight the need for direct measurement the DC conductivity of WDM.

A promising method for measuring the dielectric and electrical properties near DC is terahertz time-domain spectroscopy (THz-TDS)[11,12]. Here, the electric field of broadband THz frequency pulse is measured in time-domain, $E(t)$, and the complex-valued spectrum, $\tilde{E}(\omega)$ is obtained by a numerical Fourier transform. Analysis of changes in the spectrum of the THz pulse after reflecting or transmitting through a sample yields the complex dielectric function, $\tilde{\epsilon}(\omega)$, which can then be related to the complex conductivity. Compared with visible and near infrared frequency pulses, THz frequency pulses evolve on timescales much slower than the electron scattering time ($\tau$ ∼10-100 fs in typical metals[13], possibly shorter in WDM[9]). This makes THz frequency radiation a more appropriate probe for the near DC conductivity.

Using THz-TDS to interrogate WDM requires single-shot measurements of THz time-domain waveforms. There has been a strong effort to develop single-shot THz-TDS (SS-THz-TDS) where the THz waveform is encoded in a single laser pulse[14], and SS-THz-TDS of WDM in a reflection geometry has been reported previously[15]. However, critical density shielding makes reflectivity more sensitive to the surface conductivity and the associated electron density gradient. Furthermore, the detection method used suffers from limited time-resolution[16] and can produce artifacts[17]. While measurement of the THz transmission through WDM would provide a more accurate determination of the bulk conductivity of WDM, the small transmission expected ($t \sim 0.01$ for nanometer thick samples) means that an extremely high signal-to-noise ratio (SNR) is required. Recently, there have been significant developments in sensitive single-shot THz-TDS techniques that retain the time resolution and accuracy of conventional electro-optic sampling. In particular, using an echelon has emerged as a promising means for accurate single-shot THz detection[14,18–21].

In this paper, we present an experimental setup capable of measuring THz-time domain waveforms in a single shot with sufficient SNR for WDM experiments. The current design improves on our previously developed experimental setup which was capable measurement THz transmission through 30nm free-standing gold thin film in a single-shot[21]. We analyze the noise performance of the system and demonstrate the feasibility of measuring the bulk conductivity of WD aluminum at electron temperature ($T_e$) up to 0.5 eV .

## II. EXPERIMENTAL DESIGN

A schematic of the experimental setup is show in Fig. 1. All experiments were performed using an amplified

[a] Published as part of the Proceedings of the 22nd Topical Conference on High-Temperature Plasma Diagnostics, San Diego, California, April, 2018.

[b] Electronic mail: benofori@SLAC.stanford.edu

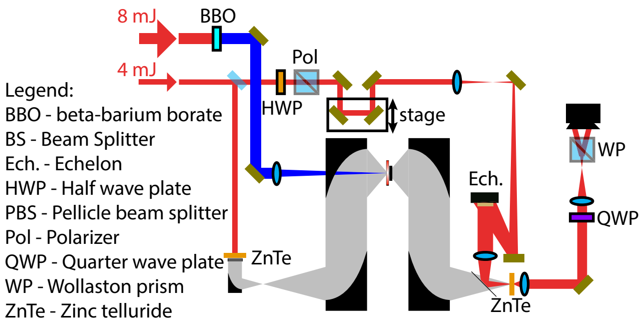


FIG. 1. Schematic of the setup used for the single-shot THz measurements described.

laser system capable of providing a pair of compressed 800 nm center wavelength, 1.55 eV photon energy, pulses with up to 5 and 8 mJ of laser energy respectively. The laser could be down-counted to single-shot mode using a Pockels cell, or also run at subharmonics of the maximum repetition rate of 120 Hz. The 8 mJ pulse was frequency doubled to 400 nm center wavelength, 3.1 eV photon energy. The conversion efficiency of the second harmonic generation was approximately 25%, and so the maximum 3.1 eV pulse energy available was 2 mJ. The beam was directed to a mechanical delay stage before being focused using an $f = 75$ cm focal length lens and directed towards the sample. The lens was placed less than the focal distance away from the sample to produce a beam diameter large enough for uniform illumination over the THz spot. Residual transmitted pump light was blocked by a 1 mm thick black teflon disc.

From the other arm of the laser, 4 mJ was available for THz generation and detection by optical rectification and electro-optic sampling[22]. The 4 mJ pulse was expanded to greater than 15 mm diameter and split with 90% of the energy used to produce THz pulses by optical rectification in a 2 mm thick $\langle 110 \rangle$ zinc telluride (ZnTe) crystal. A black 1 mm thick teflon disc placed after the ZnTe was used to filter out extra pump light. The THz pulses were focused by a 25.4 mm diameter, 50.8 mm effective focal length 90° off-axis parabolic reflector (OAP). This focus was relay imaged with a 2× demagnification using a pair of 76.2 mm diameter 90° OAPs, with effective focal lengths of 151.4 mm and 76.2 mm respectively. The resulting THz spot at the sample was focused such that $> 75\%$ of the total THz field passed through a 1 mm diameter pinhole. The focusing OAP also had a 3 mm hole for injecting the optical pump. A second pair of 76.2 mm diameter 90° off-axis OAPs with 76.2 mm and 151.4 mm focal lengths were used to relay image this focal spot onto a second 2 mm thick $\langle 110 \rangle$ ZnTe crystal which was used for free-space electro-optic (EO) sampling[23]. No part of the THz system was enclosed.

The remaining 10% of the 800 nm pulse energy was attenuated and directed into a mechanical delay stage. The beam was expanded to produce a uniform spatial profile over diameter >25.4 mm and then reflected off a 15 mm × 15 mm reflective echelon. The echelon, fabricated by Sodick F.T., consisted of 500 gold coated steps which were $W = 30.0 \pm 0.2$ $\mu$m wide and $H = 5.00 \pm 0.02$ $\mu$m tall. The thickness of the gold coating was 10 $\mu$m. As each step is large compared to the wavelength of the sampling pulse, the specular reflections from the individual steps effectively split the single input pulse into 500 distinct pulses which were time delayed by an amount

$$\Delta t = \frac{2H}{c_0 \cos(\theta)}, \tag{1}$$

where $\theta$ is the incidence angle of the beam relative to the normal of the steps of the echelon ($\theta = 0$ corresponds to the beam propagating normal to the long face of the step, not normal to the surface) and $c_0$ is the speed of light. For a 10° incidence angle, this gives a $\Delta t$ of 34 fs. The echelon was placed 100 mm in front of an $f = 100$ mm focal length lens, and the focusing beams were overlapped using a pellicle beamsplitter with the THz pulse in the ZnTe detection crystal. An $f = 30$ mm focal length objective lens was used to produce an image of the echelon. This was relay-imaged using an $f = 75$ mm focal length lens onto a single Allied Vision Manta G-201-30fps 1/1.8" monochrome charge coupled-device (CCD) camera. A quarter wave plate (QWP) with its fast axis set to 45°, and a 5° splitting angle Wollaston prism were placed in the beam path downstream of the ZnTe crystal resulting a pair of balanced images at the detector corresponding to the $s$-(+) and $p$-(-) polarization states of the readout beams.

Figure 2(a) and (b) show the polarization separated images of the echelon in the presence and absence of the THz pulse, respectively. Careful inspection of the raw images with the THz pulse present reveals intensity modulation when compared with the images collected with the THz pulse absent. These modulations appear constant along the vertical axis, and vary along the horizontal axis. As each step of the echelon, which corresponds to a different time delay, is imaged to a different horizontal location on the camera, the different horizontal positions on the detector correspond to different electro-optic sampling delays.

The intensity modulations result from the interactions of the THz pulse with the sampling pulses through the Pockels effect. Here, the THz pulse introduces a birefringence, $\Delta n$, in the ZnTe crystal. This birefringence introduces a phase shift, $\Delta\phi$, between two orthogonal polarizations. The QWP and Wollaston prism convert this phase shift into an intensity modulation such that the relative intensity change in the (+) and (-) polarizations, $\Delta I^{\pm}/I_0^{\pm}$ can be related to the THz field, $E_{\text{THz}}$, as[23]

$$\frac{\Delta I^{\pm}}{I_0^{\pm}} = \frac{I^{\pm}}{I_0^{\pm}} - 1 = \pm \sin\left(\frac{2\pi r_{41} n^3 \ell}{\lambda} E_{\text{THz}}\right), \tag{2}$$

where $I^{\pm}$ and $I_0^{\pm}$ represent the intensity of the sampling pulse in the presence and absence of the THz pulse, $r_{41}$ is the electro-optic coefficient of ZnTe, $n$ is the THz refractive index, $\ell$ is the thickness of the ZnTe crystal, and $\lambda$ is the wavelength of the sampling pulse. As equation 2 indicates, two sets of echelon images are required for extraction of the THz time-domain waveform. An example ratio image, obtained by dividing the image with the THz present by the image with the THz absent, is shown in Fig. 2(c) and gives the relative intensity modulation of

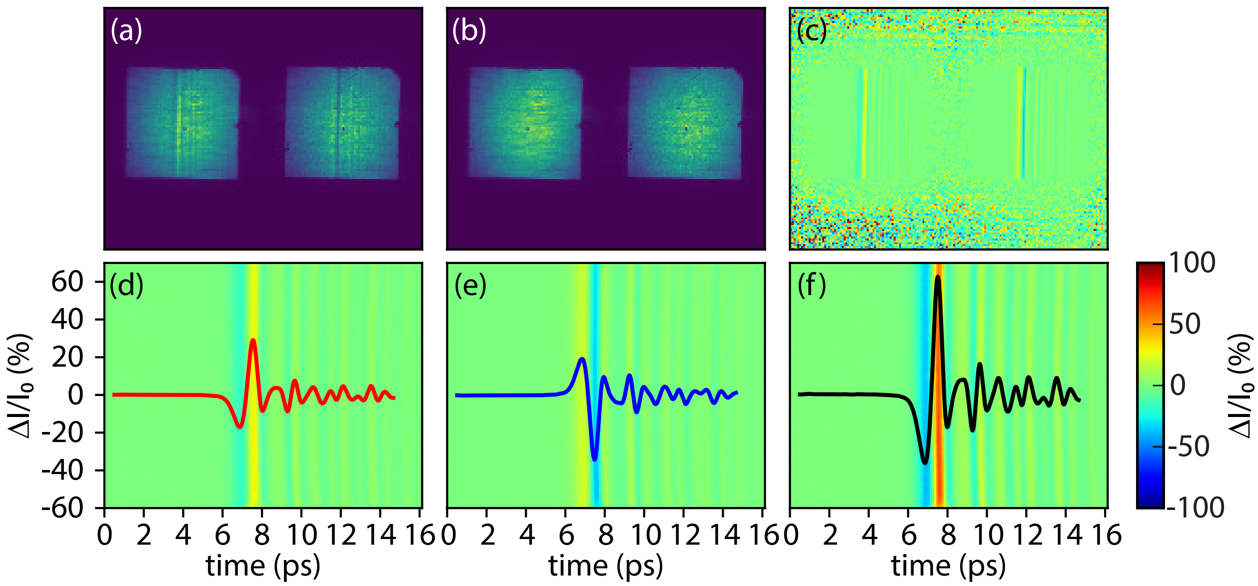


FIG. 2. Raw echelon images recorded with THz pulse (a) present and (b) absent. (c) Corresponding ratio image. Extracted THz waveforms from (d) (+)-polarization image, (e) (-)-polarization image, and (f) balanced image.

each polarization image. It can be observed that the intensity modulations are equal in magnitude but opposite in sign between the two polarization images. This can be taken leveraged to balance power fluctuations in the readout pulse: By subtracting traces obtained from the (+) and (-) ratio polarization images, power fluctuations, which appear as identical intensity variations in the ratio images, can be effectively suppressed. Furthermore, the signal is effectively doubled, and this greatly improves the signal-to-noise ratio of any single shot trace.

## III. DATA EXTRACTION PROCEDURE

In order to extract and balance the waveforms, a set of image transformation steps was required. The goal of these transformations was to map the (+) polarization image onto the (-) polarization image For convenience, these transformations were determined using an image in which the THz was absent rather than a ratio image. First, the two polarization images were cropped from the raw data using user defined boxes with width $N_x$ and height $N_y$. In order to make the cropped regions identical, a numerical cross correlation was used to determine the offset of the cropping regions with respect to the polarization images. The (-) polarization image was then shifted by an amount $(\Delta x, \Delta y)$ using a discrete Fourier Transform. The shifted image, $I^-(x-\Delta x, y-\Delta y)$, was obtained by multiplying the discrete Fourier transform of the original image, $\tilde{I}^-(u,v) = \mathcal{F}[I^-(x,y)]$ by a shifting function, $\exp\left[-i2\pi\left(u\Delta x/N_x + v\Delta y/N_y\right)\right]$ and then inverse Fourier transforming. No additional image manipulation steps were performed to get the images into register. Image registration was checked by dividing the (+) polarization image and the shifted (-) polarization image.

To retrieve the time-domain waveforms, the images need to be averaged along the vertical dimension of the echelon. Small rotations of the images were corrected by applying a numerical projective transform. Four points were selected to form a box whose sides were parallel to the edges of the echelon image. These four points were mapped to a rectangle of a specified width and height. Because the (+) and (-) polarization images had been mapped to the same points, the same transformation was applied to both images. Finally, a smaller subregion away from the edges is averaged along the vertical dimension to obtain the time-domain waveform. Example images and traces obtained for the (+) and (-) polarizations, as well as the balanced image and trace are shown in Figs. 2(d)-(f). The oscillations visible after the main cycle of the THz pulse come from absorption due to atmospheric water vapor. Here, the peak signal modulation of >60% in the balanced case is obtained because of the thick generation and detection ZnTe crystals. These thicknesses were chosen because of the long coherence length between the 800 nm pulse and the THz pulse[22]. This allows for efficient THz generation and for the full length of crystal to be used for EO sampling. Placing the setup in a dry air or nitrogen environment would also increase the signal by reducing the absorption from atmospheric water.

## IV. RESULTS

### A. Noise Characterization

In order to quantify the minimum detectable signal for the instrument, 400 single-shot images were recorded with the THz absent. The data were divided so that 200 served as "THz on" shots and 200 were "THz off" shots. These images were processed to obtain ratio images for the (+) and (-) polarizations, and balanced as well. The root-mean-square (RMS) deviation from zero was determined, and served as a measurement of the noise floor.

The results of these calculations are shown in Fig. 3.

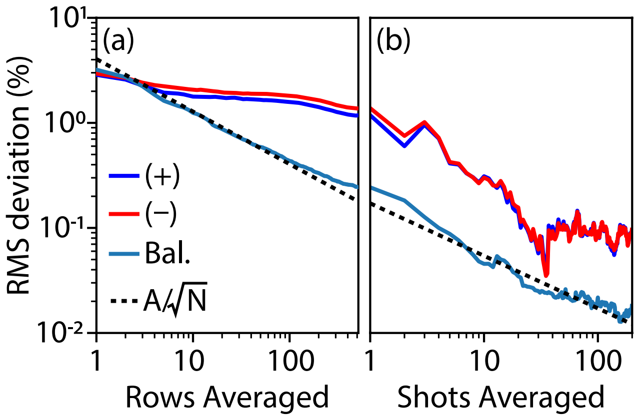


FIG. 3. Traces of the RMS deviation of the (+)-polarization, (-)-polarization, and balanced traces in (a) a single image as more rows on the detector are averaged and (b) as multiple images are averaged using the maximum number of rows available. The dashed line is proportional to $1/\sqrt{N}$ showing that the noise of the balanced trace decreases as expected.

The RMS deviation was calculated as a function of the number of rows averaged (see Fig. 3(a)) on the detector and the number of images averaged (see Fig. 3(b)) in all three cases and clearly showing the impact of averaging and balancing. Averaging more rows reduces the noise contributions arising from the electrical read noise on the CCD. Averaging shots corrects for shot-to-shot fluctuations. In both Fig. 3(a) and (b), the two polarization ratio images are strongly correlated as evidenced by their similar behavior. It is this same strong correlation that makes balancing an effective tool for noise suppression. In this case, balancing reduces the RMS deviation by almost an order of magnitude, such that the single-shot RMS deviation 0.2%. This gives a signal-to-noise ratio of $> 300 : 1$ on a single-shot trace for our system. Furthermore, there is a continued reduction in the noise by averaging single-shot traces. This indicates that even for weakly transmissive films, single-shot traces can be averaged to improve the signal-to-noise ratio.

### B. Experimental Demonstration

To demonstrate the capabilities of our system, we show single-shot waveforms of THz pulses transmitted through thin films of aluminum in the absence and presence of laser heating. The aluminum film was prepared by first depositing 40 nm aluminum onto a polished sodium chloride substrate by e-beam evaporation. Next, the sodium chloride was dissolved in distilled water, and the aluminum film was then transfered onto a 190 $\mu$m thick glass coverslip. Oxide layers about 5 nm thickness are expected on both surfaces of the aluminum[24], leaving about 30 nm thick of metallic aluminum in our sample. Measurements of the THz pulse transmitted through the bare glass (not shown) yield a peak $\Delta I/I_0$ to 33% for the balanced waveform. For all of the following measurements, the laser system was placed into single shot mode, and optical beam blocks were used to block the 400 nm

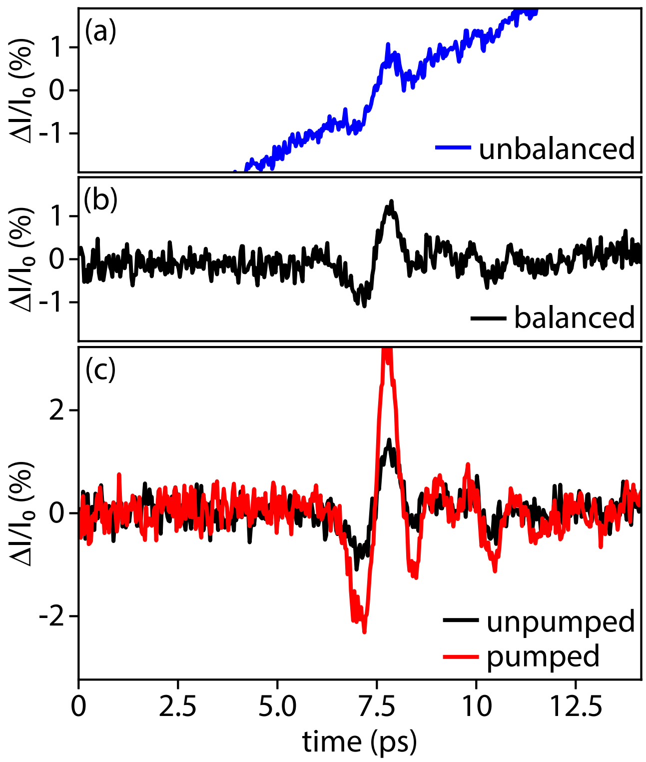


FIG. 4. Representative (a) unbalanced and (b) balanced single-shot traces of THz pulses transmitted through aluminum thin films. The effect of balancing is particularly important for measuring a small signal. (c) Waveforms of THz pulses transmitted through unpumped and pumped aluminum thin films.

pump pulse only, or both the 400 nm pump and the THz generating 800 nm pulses to collect THz only and THz absent images of the echelon for data analysis.

Figures 4(a) and 4(b) show representative unbalanced and balanced single-shot waveforms, respectively. In the absence of balancing the THz pulse can still be observed, but this is apparent only because the structure in the baseline is much more gradual than the cycle of the THz pulse. The effect of balancing is apparent as the baseline flattens and is centered around zero without any additional processing. The further increase in the signal also makes even the smaller oscillations after the main pulse visible. The balanced waveform has a peak signal modulation of 1.2%, which is still $6\times$ the noise floor of the measurement. The corresponding transmission through the aluminum film is therefore $t = 0.03$ for the unpumped film.

Figure 4(c) shows the THz transmission of the same aluminum film with and without laser excitation. In this case, a 400 nm, 50 fs (FWHM) pulse was directed through the hole in the OAP onto the film. The fluence on target was 50 mJ/cm$^2$ and the spot size was >2 mm in diameter, significantly larger than the THz spot. The time delay, which was calibrated using the optical pump-THz probe response in silicon[25], was set so that the 400 nm pulse arrived 13.3 ps prior to the THz pulse. Under these conditions, the material is expected to reach a maximum electron temperature of 0.5 eV right after heating, and then electron-ion temperature equilibrium is expected within

5 ps[26], reaching an equilibrium temperature of ∼0.1eV, just above the melting point of aluminum.

The data clearly show an increase (compare red to black in Fig. 4(c)) in the THz peak amplitude following optical pumping. In the pumped case, the peak signal modulation rises to 3.3%, corresponding to a transmission of $t = 0.097$. An estimate of the conductivity change can be made according to the Tinkham equation[27]:

$$\sigma = \frac{n_s + 1}{Z_0 d}\left(\frac{1}{t} - 1\right) \tag{3}$$

where $n_s$ is the refractive index of the substrate, $Z_0 = 377\Omega$ is the impedance of free space, $d$ is the film thickness, and $t$ is the transmission coefficient for the THz field. In this case, a 3-fold increase in the transmission implies a roughly three-fold decrease in the conductivity. Assuming the thin film expansion is negligible at excitation fluence just beyond the melting point[28] and a substrate index of $n_s = 2.5$[29], this gives a conductivity of $2.9\times10^6$ S/m after laser excitation. This value closely agrees with the conductivity of liquid aluminum measured at 0.1eV equilibrium temperature[30]. This clearly demonstrates the feasibility of using SS-THz-TDS in a transmission geometry for investigating WDM.

## V. CONCLUSION

In conclusion, we have developed and demonstrated an experimental setup capable of performing single-shot THz-TDS measurements of WDM in transmission mode. Using a reflective echelon, we can record THz time-domain waveforms in single-shot with a high SNR, and use these waveforms for spectroscopic measurements of WDM systems. Although not discussed here, the system also possesses the capability for performing time-resolved measurements using a mechanical delay stage to vary the delay between the optical pump and the THz probe, as well as measurements below the damage threshold using multi-shot averaging and differential detection techniques. These will be the subject of future investigations. To further improve the system, the entire system will be placed into a nitrogen atmosphere which will reduce absorption from atmospheric water vapor and further increase the SNR.

## ACKNOWLEDGMENTS

This work was funded by the DOE Office of Science, Fusion Energy Science under FWP 100182.

[1] A. Ng, T. Ao, F. Perrot, M. W. Dharma-Wardana, and M. E. Foord, Laser Part. Beams **23**, 527 (2005), arXiv:0505070 [physics].
[2] L. B. Fletcher, H. J. Lee, T. Döppner, E. Galtier, B. Nagler, P. Heimann, C. Fortmann, S. LePape, T. Ma, M. Millot, A. Pak, D. Turnbull, D. A. Chapman, D. O. Gericke, J. Vorberger, T. White, G. Gregori, M. Wei, B. Barbrel, R. W. Falcone, C.-C. Kao, H. Nuhn, J. Welch, U. Zastrau, P. Neumayer, J. B. Hastings, and S. H. Glenzer, Nat. Photonics **9**, 274 (2015).
[3] L. Spitzer and R. Härm, Phys. Rev. **89**, 977 (1953).
[4] Y. T. Lee and R. M. More, Phys. Fluids **27**, 1273 (1984).
[5] M. P. Desjarlais, J. D. Kress, and L. A. Collins, Phys. Rev. E - Stat. Physics, Plasmas, Fluids, Relat. Interdiscip. Top. **66**, 2 (2002).
[6] B. B. Witte, L. B. Fletcher, E. Galtier, E. Gamboa, H. J. Lee, U. Zastrau, R. Redmer, S. H. Glenzer, and P. Sperling, Phys. Rev. Lett. **118**, 1 (2017).
[7] H. M. Milchberg, R. R. Freeman, S. C. Davey, and R. M. More, Phys. Rev. Lett. **61**, 2364 (1988), arXiv:arXiv:1011.1669v3.
[8] Z. Chen, B. Holst, S. E. Kirkwood, V. Sametoglu, M. Reid, Y. Y. Tsui, V. Recoules, and A. Ng, Phys. Rev. Lett. **110**, 1 (2013).
[9] A. Ng, P. Sterne, S. Hansen, V. Recoules, Z. Chen, Y. Y. Tsui, and B. Wilson, Phys. Rev. E **94**, 4 (2016).
[10] P. Sperling, E. J. Gamboa, H. J. Lee, H. K. Chung, E. Galtier, Y. Omarbakiyeva, H. Reinholz, G. Röpke, U. Zastrau, J. Hastings, L. B. Fletcher, and S. H. Glenzer, Phys. Rev. Lett. **115**, 115001 (2015).
[11] M. Nuss and J. Orenstein, in *Millim. Submillim. Wave Spectrosc. Solids*, Vol. 12, edited by G. Grüner (1998) Chap. 2, pp. 7–50.
[12] M. Hangyo, M. Tani, and T. Nagashima, Int. J. Infrared Millimeter Waves **26**, 1661 (2005).
[13] N. W. Ashcroft and N. D. Mermin, *Solid State Physics*, 1st ed. (Brooks/Cole, Belmont, CA, 1976).
[14] S. M. Teo, B. K. Ofori-Okai, C. A. Werley, and K. A. Nelson, Rev. Sci. Instrum. **86**, 051301 (2015).
[15] K. Y. Kim, B. Yellampalle, J. H. Glownia, A. J. Taylor, and G. Rodriguez, Phys. Rev. Lett. **100**, 135002 (2008).
[16] P. Y. Han, Z. Jiang, J. A. Riordana, L. Wang, and X. Zhang, Proc. SPIE **3277**, 198 (1998).
[17] F. G. Sun, Z. Jiang, and X. C. Zhang, Appl. Phys. Lett. **73**, 2233 (1998).
[18] Y. Minami, Y. Hayashi, J. Takeda, and I. Katayama, Appl. Phys. Lett. **103**, 051103 (2013).
[19] Y. Minami, K. Horiuchi, K. Masuda, J. Takeda, and I. Katayama, Appl. Phys. Lett. **107**, 171104 (2015).
[20] G. T. Noe, I. Katayama, F. Katsutani, J. J. Allred, J. A. Horowitz, D. M. Sullivan, Q. Zhang, F. Sekiguchi, G. L. Woods, M. C. Hoffmann, H. Nojiri, J. Takeda, and J. Kono, Opt. Express **24**, 30328 (2016), arXiv:1608.08569.
[21] B. K. Russell, B. K. Ofori-Okai, Z. Chen, M. C. Hoffmann, Y. Y. Tsui, and S. H. Glenzer, Opt. Express **25**, 16140 (2017).
[22] A. Nahata, D. H. Auston, T. F. Heinz, and C. Wu, Appl. Phys. Lett. **68**, 150 (1996).
[23] P. C. M. Planken, H.-K. Nienhuys, H. J. Bakker, and T. Wenckebach, J. Opt. Soc. Am. B **18**, 313 (2001).
[24] J. Evertsson, F. Bertram, F. Zhang, L. Rullik, L. Merte, M. Shipilin, M. Soldemo, S. Ahmadi, N. Vinogradov, F. Carl, J. Weissenrieder, M. Gthelid, J. Pan, A. Mikkelsen, J.-O. Nilsson, and E. Lundgren, Applied Surface Science **349**, 826 (2015).
[25] J. Zielbauer and M. Wegener, Appl. Phys. Lett. **68**, 1223 (1996).
[26] Z. Lin, L. V. Zhigilei, and V. Celli, Phys. Rev. B **77**, 075133 (2008).
[27] M. Tinkham, Phys. Rev. **104**, 845 (1956).
[28] B. J. Siwick, J. R. Dwyer, R. E. Jordan, and R. Miller, Chemical Physics **299**, 285 (2004), ultrafast Science with X-rays and Electrons.
[29] M. Naftaly and R. E. Miles, Proc. IEEE **95**, 1658 (2007).
[30] G. R. Gathers, Reports on Progress in Physics **49**, 341 (1986).